Chemical Engineering Journal 524 (2025) 169029

Contents lists available at ScienceDirect

Chemical Engineering Journal

journal homepage: www.elsevier.com/locate/cej

Synergistic enhancement of Raney-Ni catalyst for methane dry reforming via electrochemically engineered CoNi co-catalyst

Judit Lloreda [a,b,c], Isabel Serrano [d], Jordi Llorca [d], Vanessa Abad [c], Elvira Gómez [a,b], Albert Serrà [a,b,*]

[a] Thin-film and Nanostructure electrodeposition Group (GE-CPN), Department of Material Sciences and Physical Chemistry, Universitat de Barcelona, Martí i Franquès, 1, E-08028, Barcelona, Spain
[b] Institute of Nanoscience and Nanotechnology (IN^{2}UB), Universitat de Barcelona, Martí i Franquès, 1, E-08028, Barcelona, Spain
[c] Consorci per a la Gestió dels Residus del Vallès Oriental, Camí Ral s/n, E-08401, Granollers, Spain
[d] Institute of Energy Technologies and Department of Chemical Engineering, Universitat Politècnica de Catalunya, BarcelonaTech, Campus Diagonal Besós-EEBE, E-08019, Barcelona, Spain

ARTICLE INFO

Keywords:
Raney-Ni
CoNi co-catalyst
Biogas
Dry reforming of methane
Coke deposition

ABSTRACT

Dry reforming of methane (DRM) offers a promising route to convert biogas into syngas while capturing CO_2. However, the harsh reaction conditions (≥700 °C) lead to rapid deactivation of conventional Ni-based catalysts due to carbon deposition and sintering. In this work, we explore the catalytic behavior of commercial Raney-Ni for DRM and introduce electrochemically synthesized CoNi microparticles as co-catalysts to enhance stability and performance. Catalyst screening was performed in a fixed-bed reactor using a CH_4:CO_2:N_2 = 3:2:10 feed mixture under atmospheric pressure. Raney-Ni showed high activity (CH_4 conversion >92 % at 700 °C), but suffered from coke accumulation and deactivation after 5 h of continuous operation. CoNi–Raney-Ni composites were prepared via physical blending of CoNi and Raney-Ni powders, and tested at various compositions. The best-performing among the tested compositions (25 wt% CoNi) maintained high conversion (>90 %) and stable syngas production (H_2/CO ≈ 1.0) over extended periods. Post-reaction analysis revealed extensive filamentous carbon on pure Raney-Ni, while CoNi-containing catalysts exhibited smoother surfaces and suppressed graphitic carbon, as confirmed by FE-SEM and Raman spectroscopy. Notably, CoNi alone showed minimal CH_4 activation but enhanced CO_2 dissociation and limited carbon formation. These results demonstrate a synergistic effect, where CoNi promotes carbon gasification while Raney-Ni provides high CH_4 reactivity. This composite approach enables scalable, low-cost catalysts with improved coke tolerance for biogas reforming applications.

1. Introduction

The global shift toward low-carbon energy systems has intensified the search for scalable, sustainable hydrogen production technologies [1,2]. Hydrogen is widely recognized as a cornerstone of the energy transition due to its high energy density, zero carbon emissions at the point of use, and cross-sectoral versatility. However, more than 95 % of global hydrogen currently produced from fossil fuels via steam reforming of methane (SRM) or coal gasification – processes associated with significant CO_2 emissions [3–5]. Although water electrolysis powered by renewable energy is carbon-neutral, its development remains constrained by high energy demands, infrastructure costs, and freshwater availability [6–8].

As a decentralized and waste-derived alternative, biogas valorization is gaining attention as a pathway to renewable hydrogen [9–11]. Biogas, generated through the anaerobic digestion of organic waste matter, typically comprises 45–70 vol% CH_4 and 30–55 vol% CO_2, with trace contaminants such as H_2S, VOCs, and siloxanes. Its composition depends on the feedstock, ranging from agricultural residues to municipal solid waste or sewage sludge [12,13]. With European regulations now prohibiting the landfilling of biodegradable waste, biological treatment is increasingly adopted [14,15]. In Catalonia, 3.77 million tons of municipal waste were collected in 2023, with 11.6 % identified as organic [16]. Among the region's treatment facilities, the *Vallès Oriental*

* Corresponding author at: Thin-film and Nanostructure electrodeposition Group (GE-CPN), Department of Material Sciences and Physical Chemistry, Universitat de Barcelona, Martí i Franquès, 1, E-08028, Barcelona, Spain.
E-mail address: a.serra@ub.edu (A. Serrà).

https://doi.org/10.1016/j.cej.2025.169029
Received 17 July 2025; Received in revised form 19 September 2025; Accepted 27 September 2025
Available online 29 September 2025

Waste Treatment Centre (CGRVO) has produced biogas since 2009. While currently used for electricity and heat generation, this gas represents an untapped hydrogen source. A detailed summary of seasonal biogas composition at CGRVO is provided in the Supporting Information (Table S1).

Among thermochemical routes for biogas upgrading, dry reforming of methane (DRM) stands out as a direct conversion of CH_4 and CO_2 into syngas (Eq. 1), offering both carbon capture and utilization (CCU) benefits [17–21]. Syngas can serve as a precursor for methanol synthesis, Fischer–Tropsch fuels, or hydrogen via water–gas shift reactions [22–24].

$$CH_4 + CO_2 \leftrightarrows 2H_2 + 2CO \qquad \Delta H^0 = 247\ kJ{\cdot}mol^{-1} \tag{1}$$

Despite its advantages, DRM is strongly endothermic and requires temperatures of 600–1000 °C to activate CH_4 and CO_2, whose dissociation energies are 435 and 526 $kJ{\cdot}mol^{-1}$, respectively [25]. These harsh conditions favor secondary reactions such as methane cracking and the Boudouard reaction, leading to carbon deposition and catalyst deactivation [26].

Catalyst deactivation in DRM is primarily caused by coke formation, sintering, and structural degradation. Filamentous carbon species, though less stable than graphitic forms, can still accumulate over time and impair active site accessibility [27]. Furthermore, at elevated temperatures, nickel nanoparticles - a common DRM catalyst - tend to agglomerate and lose surface area [28]. Extensive research has thus focused on the development of stable, coke-resistant catalysts that can maintain activity over extended operation periods [29–33].

Nickel-based catalysts are the most widely studied due to their favorable balance between cost and activity [34,35]. However, conventional Ni catalysts supported on Al_2O_3, SiO_2, TiO_2, or MgO often suffer from deactivation due to carbon accumulation and sintering [36]. To address these challenges, numerous strategies have been explored, including the use redox-active supports (e.g., La_2O_3, CeO_2), promoter elements, or bimetallic systems [37–39]. In such configurations, methane activation typically occurs at the metallic sites, while CO_2 activation is facilitated by the support or co-catalyst [40,41]. Bimetallic catalysts, in particular, offer synergistic effects that improve dispersion, alter electronic properties, and enhance oxygen mobility.

Raney-Ni, a high-surface-area nickel alloy widely used in hydrogenation and biomass conversion [42,43], offers attractive properties for DRM, including thermal robustness and scalability. However, its known tendency to promote methane decomposition can lead to coke accumulation and unbalanced H_2/CO ratios [44,45]. If carbon formation can be effectively mitigated, Raney-Ni may offer a cost-effective alternative for DRM under biogas-relevant conditions.

One promising strategy is the introduction of a second transition metal to form a bimetallic system [46]. Cobalt, in particular, has demonstrated strong oxygen affinity, promoting carbon oxidation and suppressing the formation of graphitic species [47,48]. Co also enhances thermal stability and modifies the electronic environment of nickel. While noble metals like Rh or Ru offer high activity, their cost limits scalability [49]. Co—Ni systems present a more practical solution [50,51], especially when compositional control is achieved through electrochemical synthesis. In particular, electrodeposition is a versatile method to prepare bimetallic catalysts with tunable metal ratios, surface morphology, and particle size [52,53]. These characteristics are critical for tailoring catalytic behavior and understanding structure–activity relationships.

In this study, we systematically evaluate the performance of commercial Raney-Ni as a DRM catalyst, optimizing key parameters including reactor configuration, gas flow rate, and catalyst loading. To overcome limitations related to carbon accumulation, we introduce CoNi bimetallic co-catalysts synthesized via electrochemical deposition and blended with Raney-Ni. The resulting composite catalysts are benchmarked against Raney-Ni alone, and their activity, selectivity, and stability are assessed under biogas-representative conditions. Post-reaction characterization provides further insights into catalyst deactivation and recovery strategies.

2. Experimental section

2.1. Materials and reagents

All chemical reagents were of analytical grade and used without further purification. Commercial Raney-Ni (Type 2800, 50 wt% slurry in water) and fluorine tin oxide-coated glass substrates (FTO, sheet resistance 10–15 Ω $sq.^{-1}$) were purchased from Sigma-Aldrich. Nickel(II) chloride hexahydrate ($NiCl_2{\cdot}6H_2O$, 99 %) was obtained from Supelco, cobalt(II) chloride hexahydrate ($CoCl_2{\cdot}6H_2O$, 99 %) from Alfa Aesar, and boric acid (H_3BO_3, 99.5 %) from Merck. Hydrochloric acid (HCl, 37 %) was purchased from PanReac AppliChem. Quartz wool (average fiber diameter ~4 μm) and silicon carbide (SiC, 46 grit) were obtained from Thermo Scientific. Ultrapure water (18.2 MΩ cm at 25 °C) was produced using a Milli-Q system.

2.2. Optimization of reaction parameters of Raney-Ni catalyst

The catalytic performance of commercial Raney-Ni for the DRM was systematically evaluated under various reaction conditions to identify the optimal operating parameters. Experiments were conducted in a Swagelok stainless-steel tubular fixed-bed reactor (i.d. 13 mm; length 75 mm) housed in a programmable tubular furnace (Carbolite) with PID control. A quartz liner was inserted to minimize wall effects and ensure thermal homogeneity. All tests were performed at atmospheric pressure.

Before each test, the catalyst was subjected to reduction treatment under a 10 % H_2 in N_2 gas stream (50 $mL{\cdot}min^{-1}$) at 600 °C for 1 h (heating rate: 10 °$C{\cdot}min^{-1}$). The reactor was then purged with N_2 (100 $mL{\cdot}min^{-1}$) for 45 min to remove residual hydrogen. The feed gas mixture (N_2:CH_4:CO_2 = 10:3:2) included N_2 as an internal standard for chromatographic quantification.

Catalyst testing was first conducted over 600–800 °C in 100 °C increments to capture overall activity and selectivity trends. Each temperature step was maintained for 45 min. Although coarse, this interval allowed rapid screening of catalyst's thermal response. Further experiments explored:

- Catalyst bed configuration: Raney-Ni catalyst was (i) layered on four quartz wool plugs or (ii) diluted with 3.0 g of SiC (46 grit) to improve thermal conductivity and minimize pressure drop.
- Total gas flow rate: Adjusted between 80, 100, and 120 $mL{\cdot}min^{-1}$ to assess space velocity effects.
- Catalyst mass loading: Varied from 0.25 g to 1.00 g to evaluate the influence of catalytic mass on conversion.
- Catalyst stability: performed at 700 °C for 5 h under optimized conditions.

Reactor effluents were analyzed online using a micro gas chromatograph (490 Micro GC from Agilent Technologies) equipped with a molecular sieve 5 Å and a PoraPlot U column. Gas composition was recorded every 4 min. Conversions, selectivities, H_2/CO ratios, and product yields were calculated using standard equations (eqs. S1–S7, Supporting Information). Each catalyst composition was assessed in a single temperature-programmed experiment; hence no replicate statistics are provided. After each experiment, the reactor was cooled under N_2 flow to room temperature, and the spent catalyst was collected for post-reaction characterization.

2.3. Catalytic testing of CoNi–Raney-Ni composite catalysts

The CoNi co-catalyst was synthesized by potentiostatic electrodeposition from a CoNi chloride bath, followed by mechanical processing

into powders. Composite catalysts were prepared by physically mixing Raney-Ni and CoNi in different proportions. Full experimental details are provided in the Supporting Information.

Catalytic performance of the composite materials was assessed using the same Swagelok stainless-steel tubular fixed-bed reactor and operating conditions as described for Raney-Ni benchmarking. Each catalyst composition was tested once in a single temperature-programmed run; therefore, replicate statistics are not available. The study's objective was to establish the CoNi-assisted synergy (coke control and sustained activity) under biogas-relevant DRM, not to exhaustively optimize composition or resolve small H_2/CO differences. Each 700 mg catalyst sample was supported within four layers of quartz wool to ensure uniform gas-solid contact. Prior to reaction, all samples were subjected to the standard activation procedure: reduction under a 10 vol% H_2 in N_2 (50 mL·min^{-1}) at 600 °C for 1 h, followed by purging under N_2 (100 mL·min^{-1}) for 45 min.

The dry reforming of methane was conducted using a reactant mixture with a molar ratio of N_2:CH_4:CO_2 = 10:3:2 at a total flow rate of 120 mL·min^{-1}, to reach a gas hourly space velocity (GHSV) of 4800 h^{-1}. Reaction temperature was varied between 600 and 800 °C in 50 °C increments, with each step maintained for 25 min. This refined temperature interval allowed improved resolution in performance comparison while reducing total experimental time relative to earlier 100 °C increments.

Catalyst durability was evaluated by performing long-term stability tests on the best-performing composite at 700 °C for 7 h under identical gas flow and composition.

The gaseous effluent from the reactor was analyzed on-line using a micro gas chromatograph (490 Micro GC from Agilent Technologies) equipped with a molecular sieve 5 Å and a PoraPlot U column. Product distribution, conversion, selectivity, H_2/CO ratio, and product yields were calculated using the same procedure and equations described in Section 2.2.

2.4. Spent catalyst characterization

The morphology, composition, and carbon deposition characteristics of the fresh and spent catalysts were thoroughly investigated using a combination of microscopic and spectroscopic techniques.

Field emission scanning electron microscopy (FE-SEM) images were acquired using a JEOL JSM-7100F microscope operated at 20 kV and equipped with an Oxford Instruments X-MaxN 80 energy-dispersive X-ray spectroscopy (EDS) detector. Representative surface regions were selected by analyzing at least eight different randomly chosen zones per sample to ensure statistical relevance. EDS was used to confirm elemental composition and homogeneity of the CoNi particles, with particular attention to the Co/Ni atomic ratio and metal dispersion on the catalyst surface.

Raman spectra of spent catalysts were collected to assess carbon deposition and character of surface carbon species. Measurements were carried out using a dispersive spectrometer Jobin-Yvon LabRam HR 800, coupled to an optical microscope Olympus BXFM, in the 200–3000 cm^{-1} range employing a green laser (523 nm) and calibrated using a silicon reference at 520.7 cm^{-1}. Each spectrum was obtained by averaging five accumulations. Baseline correction and D/G band fitting procedures were conducted using the instrument's integrated software. D/G intensity ratios were extracted to estimate the relative amount and structure of the carbonaceous deposits. Finally, X-ray powder diffraction (XRD) measurements were performed on a Bruker D8 Advance diffractometer in Bragg–Brentano geometry using Ni-filtered Cu Kα radiation (λ = 1.5418 Å; 45 kV, 40 mA) and 0.04 rad Soller slits. Diffraction patterns were collected over the 2θ range 20–100° with a step size of 0.02° and a dwell time of 1 s per step.

3. Results and discussion

3.1. Optimization of reaction parameters of Raney-Ni catalyst

Raney-Ni is a well-known, non-noble metal catalyst widely used in hydrogenation and biomass upgrading due to its high surface area, porosity, and intrinsic activity [54]. However, its application in methane dry reforming has received limited attention, especially under conditions relevant to biogas. In this study, a systematic evaluation of commercial Raney-Ni was undertaken to assess its viability and optimize the operational parameters for DRM.

Given the intended application in biogas reforming, careful consideration was given to the selection of the feed gas composition in order to emulate realistic operating conditions. Biogas typically consists of 45–70 % methane and 30–55 % carbon dioxide, along with trace levels nitrogen, hydrogen, sulfide, and water vapor [12]. To reflect an average composition while maintaining experimental control, a CH_4:CO_2 molar ratio of 60:40 was chosen. This ration provides a representative scenario for biogas valorization while allowing meaningful assessment of catalyst performance under relevant reactant proportions. In addition, nitrogen was incorporated as an inert internal standard and diluent, resulting in a final feed gas composition of N_2:CH_4:CO_2 = 10:3:2. This corresponds to 66.7 % N_2, 20.0 % CH_4, and 13.3 % CO_2 by volume. The inclusion of nitrogen serves two purposes: (i) enabling accurate quantification of reactant conversions and product yields by acting as a non-reactive reference in gas chromatography, and (ii) moderating the overall reactivity of the gas stream to prevent catalyst overheating or mass transfer limitations during dry reforming.

Initial catalytic tests were performed using 0.25 g of Raney-Ni at 600, 700, and 800 °C. As expected, both methane and carbon dioxide conversion increased with temperature (Fig. 1a), confirming the endothermic nature of the DRM reaction ($\Delta H^\circ = +247$ kJ·mol^{-1}) [55]. At 800 °C, CO_2 conversion exceeded 96 %, while CH_4 conversion remained slightly lower (~91 %), consistent with thermodynamic limitations and side reactions.

Syngas composition, monitored throughout the reaction, showed that the H_2/CO ratio remained above 1 at all temperatures, with a decreasing trend as temperature increased (Fig. S1). This suggests the concurrent contribution of methane decomposition ($CH_4 \rightarrow C + 2H_2$), especially at higher temperatures. The elevated H_2/CO ratios observed are beneficial for hydrogen-enriched syngas applications but may exacerbate coke formation.

The effect of bed configuration, flow rate, and catalyst mass was systematically studied to identify the work conditions (Figs. 1 and S1, and Table S2). A detailed discussion of these optimization studies is provided in the Supporting Information (Section SI-3). Quartz wool proved superior to SiC, yielding consistently higher conversions and more stable operation. This was attributed to better catalyst dispersion, uniform temperature distribution, and improved gas–solid contact. In contrast, the SiC configuration suffered from local carbon accumulation and faster deactivation.

Gas hourly space velocity strongly influenced performance. Lower flow rates (80 mL·min^{-1}) provided higher conversions due to longer residence times but promoted secondary reactions such as methane cracking and reverse water–gas shift, resulting in increased coke deposition. At 120 mL·min^{-1}, conversions were slightly lower but hydrogen productivity per gram of catalyst was maximized, and coke formation was reduced, making this the most favorable condition.

Catalyst mass loading mainly affected stability rather than overall productivity. Although total H_2 production (~1750 μmol·min^{-1} at 700 °C) was nearly constant across 0.25–1.00 g loadings, higher mass improved stability by distributing carbon over more active sites, delaying deactivation, and producing more uniform coke deposits. Consequently, 1.00 g of Raney-Ni provided the best balance between activity and durability.

Overall, the optimization study established 700 °C, 120 mL·min^{-1},

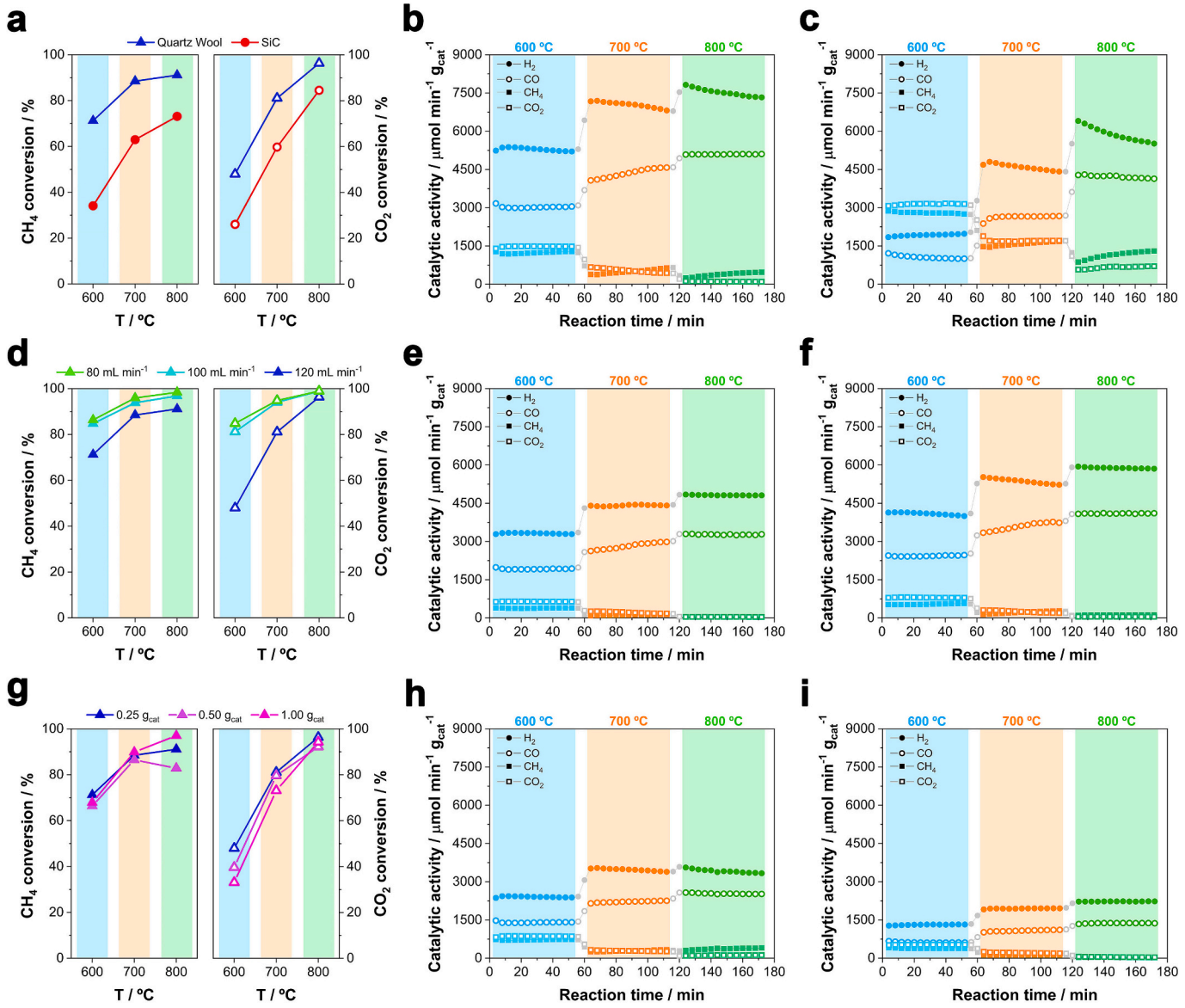

Fig. 1. (a) CH_4 and CO_2 conversions and catalytic activity evolution for (b) quartz wool and (c) SiC supports during catalyst bed configuration tests. (d) CH_4 and CO_2 conversions and catalytic activity evolution for (e) 80 mL·min^{-1}, (f) 100 mL·min^{-1} and (b) 120 mL·min^{-1} gas flows during gas flow rate tests. (g) CH_4 and CO_2 conversions and catalytic activity evolution for (b) 0.25 g, (h) 0.50 g and (i) 1.00 g of Raney-Ni during catalyst mass loading tests.

and 1.00 g Raney-Ni supported on quartz wool as the baseline operating conditions. These results highlight not only the catalytic potential of Raney-Ni under biogas-relevant DRM but also the key process parameters governing stability and coke tolerance, which serve as a critical reference point for evaluating the synergistic effects of the CoNi–Raney-Ni composite catalysts.

3.2. *Catalytic performance of CoNi–Raney-Ni composite catalysts*

Electrochemically engineered CoNi microparticles were synthesized by potentiostatic electrodeposition on FTO substrates, followed by mechanical detachment and sonodispersion. The process yielded near-equimolar Co/Ni compositions and microparticles with rough, high-surface-area morphologies, consistent with the formation of porous metallic frameworks. Composite catalysts were then prepared by low-temperature physically blending CoNi powders with commercial Raney-Ni at fixed total mass (700 mg) and varying CoNi contents (25–65 wt%) without calcination, followed by the same in-situ reduction as the baseline catalyst, to preserve the skeletal texture of Raney-Ni and the CoNi particle morphology and to minimize pre-reaction sintering. Representative SEM/EDS analyses confirmed the preservation of the characteristic porous texture of Raney-Ni and the uniform distribution of Co and Ni within the composites, without evidence of macroscopic segregation. This preparation strategy ensures intimate mixing between Raney-Ni, which primarily promotes CH_4 activation, and CoNi, which facilitates CO_2 activation and carbon suppression, thereby enabling cooperative effects in DRM. Full experimental details, including electrodeposition conditions, voltammetric analysis, particle size distribution, and comprehensive structural characterization, are provided in the Supporting Information (Sections SI-5 and SI-6).

Catalytic experiments were conducted to evaluate the performance of the CoNi–Raney-Ni composites in the DRM. For all tests, the total catalyst mass was fixed at 700 mg, ensuring a consistent gas hourly space velocity (GHSV = 4800 h^{-1}) across all samples. Prior to testing the composite formulations, the individual catalytic behavior of the electrochemically synthesized CoNi powder was evaluated under identical conditions to establish a reference for intrinsic activity.

As shown in Fig. S8a, the CoNi microparticulate catalyst exhibited

negligible activity at temperatures below 700 °C. Upon increasing the temperature, moderate conversion of CO_2 and CH_4 was observed, with a strong selectivity toward CO over H_2. The H_2/CO ratio remained consistently below 1 throughout the entire temperature range, and CO_2 conversion was approximately twice that of CH_4. These results suggest that the CoNi catalyst predominantly facilitates CO_2 activation pathways – likely via dissociative adsorption and reverse water-gas shift – while showing limited efficacy in methane activation. The absence of substantial H_2 formation further supports the conclusion that methane dehydrogenation, which is typically associated with carbon formation, is not a favored pathway over this material. In contrast, pure Raney-Ni demonstrated significantly higher activity across the entire temperature range (Fig. S8b). High CH_4 and CO_2 conversions were achieved even at low temperatures, with H_2/CO ratio exceeding unity at all the tested points. This confirms the prominent role of methane decomposition on the Raney-Ni surface, which promotes elevated H_2 yields but also increases the propensity for the coke formation, as previously discussed in Section 3.1.

To evaluate the influence of CoNi content on DRM performance, the previously prepared composite catalysts (C1–C4) were tested under identical conditions (Fig. 2). Each catalyst was evaluated with a fixed total mass of 700 mg, ensuring consistent GHSV across all tests, while varying only in the relative weight fraction of Raney-Ni to CoNi (35:65 for C1 to 75:25 for C4). The reaction temperature was increased in 50 °C intervals, providing a comparative evaluation of catalyst behavior across a relevant temperature range.

The most CoNi-rich catalyst, C1 (65 wt% CoNi), exhibited the lowest overall activity and stability (Fig. 2a). This lack of stability regarding the decrease in hydrogen production, especially during the 650 and 700 °C reaction temperatures, goes alongside an increase in CH_4 concentration, meaning that the decomposition of methane suffers deactivation. This shows that despite the effect of Raney-Ni regarding catalytic activity, the abundant presence of CoNi in the composite has a significant inhibitory effect. At higher temperatures a certain stability is regained, overlapping with the beginning of catalytic activity attributed to CoNi. Despite its limited reactivity toward DRM and methane activation, it contributes to the removal of the carbonaceous deposits presumably formed, according to the behavior of Raney-Ni previously determined. When lowering the CoNi concentration to 50 % in composite C2 (Fig. 2b), the same effect regarding stability could be observed. The higher proportion of Raney-Ni ensured enhanced CH_4 and CO_2 conversions, particularly at intermediate temperatures. The improved reactivity is attributed to the

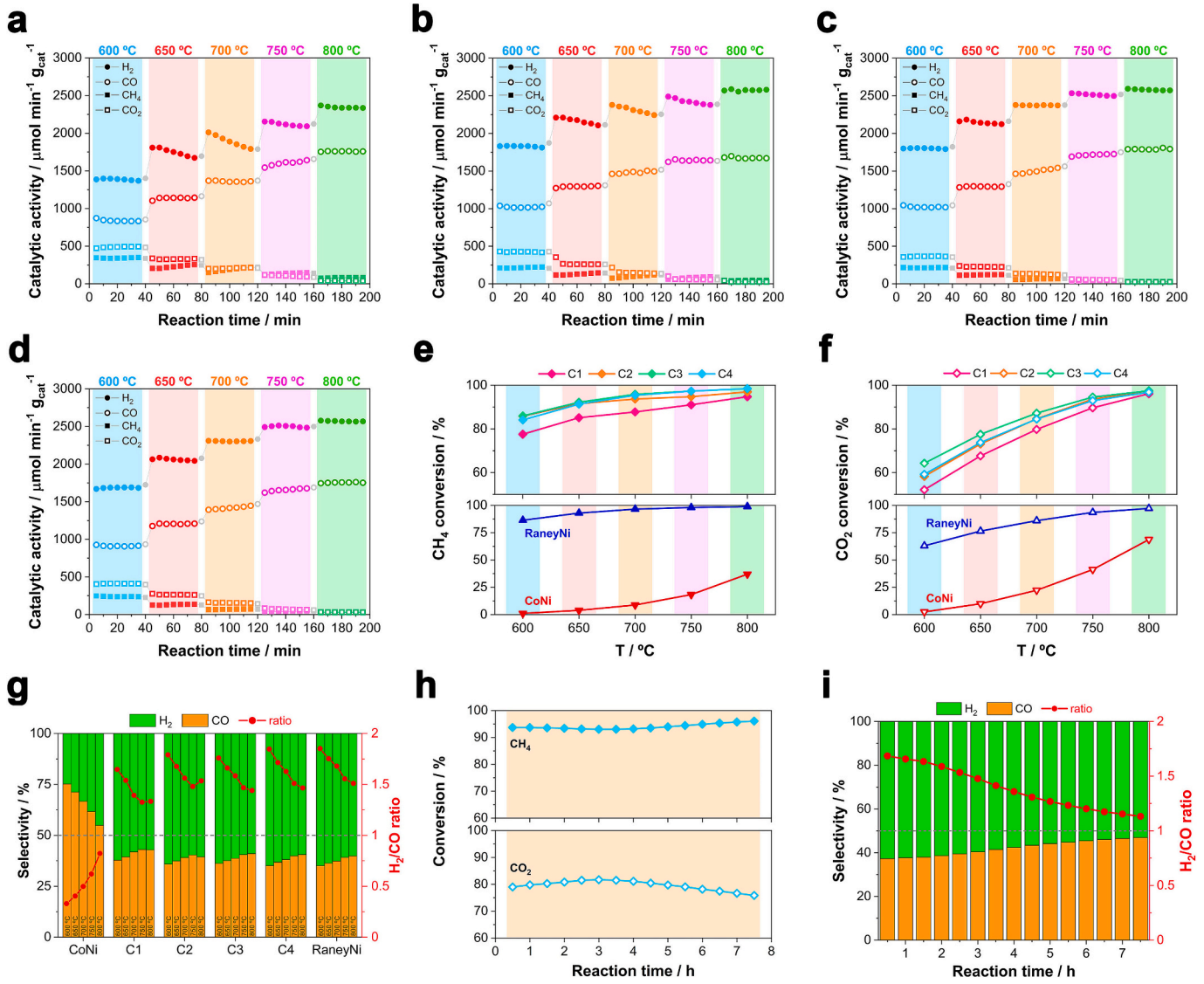

Fig. 2. Temperature effect on the catalytic activity during DRM for (a) C1, (b) C2, (c) C3, and (d) C4 catalysts, and evolution of (e) CH_4 and (f) CO_2 conversion, and of (g) the H_2 and CO selectivity and H_2/CO ratio of the composite catalysts. Evolution of (h) CH_4 and CO_2 conversion, and of (i) the H_2 and CO selectivity and H_2/CO ratio of composite catalysts C4 during the stability test (gas flow 120 mL min^{-1}, m_{cat} = 700 mg, quartz wool as catalyst support, GHSV = 4800 h^{-1}).

increased density of active Ni sites, compensating for the limited role of CoNi. However, C2 still did not match the performance of the lower-CoNi composites in terms of H_2 production and stability. Further reductions in CoNi content to 35 wt% (C3) and 25 wt% (C4) resulted in substantial gains in both activity and durability, with catalytic performance closely resembling that of pure Raney-Ni (Fig. 2c and d). Both C3 and C4 catalysts achieved high CH_4 and CO_2 conversions across the full temperature range (Fig. 2e and f), likely due to a marginally higher amount of Ni surface area available for methane decomposition. Above 700 °C, both C3 and C4 converged in performance, reaching nearly identical levels of conversion and syngas selectivity. One of the key observations across these tests was the evolution of the H_2/CO ratio, which approached 1.0 during the higher temperature stages for both C3 and C4. This ratio is indicative of a more balanced syngas composition, suitable for downstream applications such as Fischer-Tropsch synthesis or methanol production. A subtle decline in H_2 production toward the end of the reaction sequence suggested that methane decomposition remained active and that some carbon accumulation may still occur. Quantitative results for conversion, selectivity, and H_2/CO ratios are summarized in Fig. 2g and tabulated in Table S4. Nevertheless, no signs of rapid deactivation were observed over the timescale of the experiments, underscoring the durability advantages of the CoNi–Raney-Ni composite catalysts, particularly at CoNi loadings of $\leq$ 35 wt%.

These findings demonstrate that controlled incorporation of CoNi ($\leq$ 35 wt%) into Raney-Ni provides clear benefits in terms of catalyst durability and CO_2 utilization, without compromising overall activity. The partial suppression of methane decomposition, coupled with enhanced CO production, suggests that CoNi serves as an effective co-catalyst, promoting CO_2 dissociation and possibly contributing to in-situ carbon gasification, thereby delaying catalyst deactivation. Based on this performance, composite C4 (25 wt% CoNi), was selected for further post-reaction characterization and mechanistic studies aimed at understanding carbon mitigation pathways.

The performance enhancement of the CoNi–Raney-Ni composites is attributed to a bifunctional, interfacial mechanism: Raney-Ni provides efficient CH_4 activation (but generates C*), whereas CoNi preferentially activates CO_2 to supply O* that gasifies C* at CoNi|Ni contacts (C* + O* → CO) [56,57]. This cooperation sustains CH_4/CO_2 conversions, shifts H_2/CO toward unity, and slows deactivation. The effect is composition-dependent, with intermediate CoNi loadings maximizing interfacial O* supply without diluting Ni sites. The following section tests this interpretation against ex-situ evidence.

3.3. Catalyst characterization

To elucidate the mechanisms underlying catalyst deactivation and to clarify the role of CoNi in mitigating carbon accumulation, post-reaction characterizations of the spent catalysts were carried out using FE-SEM and Raman spectroscopy. Analyses were conducted on spent CoNi, Raney-Ni, and CoNi–Raney-Ni composite catalysts (C1–C4) to evaluate morphological changes, carbon nature, and the extent of carbon deposition after DRM operation.

FE-SEM micrographs of the spent CoNi catalyst (Fig. 3a and b) revealed moderate particle agglomeration, attributable to thermal sintering under high-temperature DRM conditions. Notably, no filamentous carbon structures – such as CNTs – were observed on the catalyst surface or on the surrounding quartz wool fibers. In contrast to the carbon-rich surfaces typically seen in spent Raney-Ni samples, the CoNi particles retained a relatively smooth morphology after reaction, suggesting a low degree of carbon deposition.

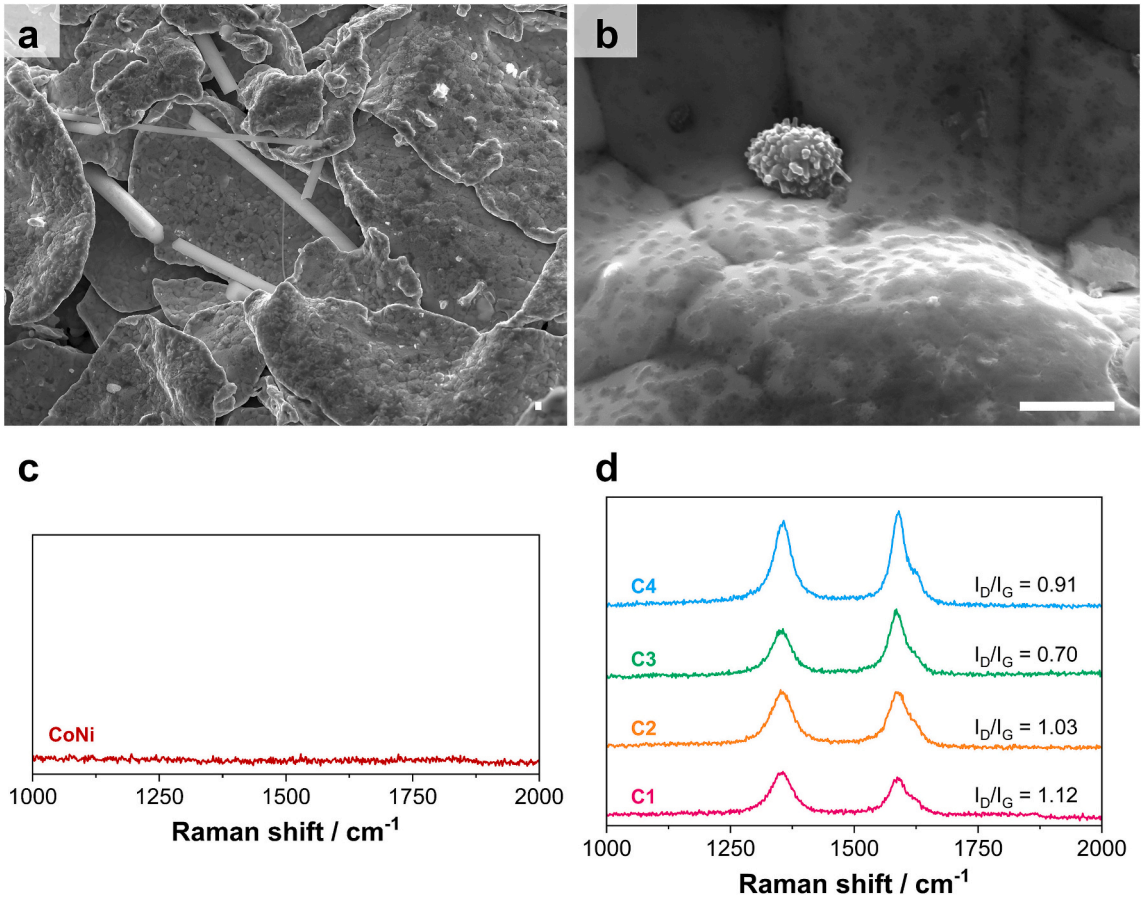

Fig. 3. Characterization of spent composite catalysts (a) and (b) FE-SEM micrographs of CoNi. Scale bar: 1 μm, and Raman spectra from (c) CoNi and (d) composites C1, C2, C3, and C4.

Raman spectroscopy further confirmed the absence of graphitic or disordered carbon on the spent CoNi catalyst (Fig. 3c). The characteristic D-band (~1360 cm^{-1}) and G-band (~1590 cm^{-1}), commonly associated with amorphous and graphitic carbon species, respectively, were not detected. This supports the conclusion that CoNi exhibits minimal susceptibility to coking under DRM conditions. These observations are consistent with the poor methane activation performance of CoNi and its preferential promotion of CO_2 dissociation pathways, which likely facilitate carbon gasification rather than formation.

The spent composite catalysts were also analyzed by FE-SEM to assess morphological evolution and carbon deposition behavior (Fig. 4). All samples exhibited varying degrees of thermal agglomeration, but more importantly, significant surface roughening and carbon filament formation were observed, especially in composites with higher Raney-Ni content. In particular, composites C3 and C4, which contained 35 wt% and 25 wt% CoNi, respectively, displayed abundant CNT-like structures (Fig. 4f and h), indicative of active methane decomposition and structured carbon formation. By contrast, composites C1 and C2, with higher CoNi content, exhibited fewer and less-developed carbon filaments, reinforcing the view that CoNi suppresses carbon nucleation and growth.

Complementary Raman analysis (Fig. 3d) confirmed the presence of carbonaceous species across all composites, with the D and G bands clearly detected. The relative intensity ratio (I_D/I_G) offers insight into the structural order of the deposited carbon. Composite C1, with the highest CoNi content, exhibited a $D/G > 1$, indicative of amorphous, disordered carbon, which is generally more reactive and more easily removed via gasification [58]. In contrast, C4, which had the highest Raney-Ni fraction, showed a $D/G < 1$, suggesting the presence of more ordered, graphitic carbon, such as CNTs. These findings correlate with FE-SEM observations and validate the hypothesis that CoNi disrupts graphitization, reducing the crystallinity of deposited carbon and thereby improving its reactivity toward removal.

To gain deeper insight into long-term structural evolution, the spent C4 catalyst was further analyzed after the 7.5-h stability test at 700 °C. FE-SEM images (Fig. 5a and b) confirmed sustained particle agglomeration, and extensive filamentous carbon deposition – predominantly in the form of CNTs – was evident on the catalyst surface, particularly on Raney-Ni particles.

Elemental mapping (Fig. 5c) demonstrated preferential carbon accumulation on Raney-Ni regions relative to CoNi zones, supporting the conclusion that Co-rich domains limit carbon deposition by promoting CO_2 activation and carbon gasification. Raman spectra of the spent C4 catalyst after prolonged operation (Fig. 5d) showed a I_D/I_G ratio close to 1.0, reflecting a more balanced mixture of disordered and graphitic carbon than observed after short-term test (I_D/I_G of 0.91). This shift in carbon character suggests a dynamic restructuring process, whereby CoNi moderates carbon accumulation even under prolonged high-conversion DRM conditions.

XRD patterns of fresh and spent catalysts (Fig. 5e and g) show three dominant reflections for Raney-Ni and the CoNi–Raney-Ni composite at ~31°, ~47°, and ~ 53. The CoNi powder displays the same set of reflections slightly shifted to higher angles (~32°, ~48°, ~53–54°), indicating a small decrease in average d-spacing consistent with alloying/strain effects in the Co-containing phase. Within the resolution of our measurements, the diffractograms remain unchanged after the five-temperature study and after the long-term stability test, with no new reflections attributable to bulk oxide or spinel phases. This evidences good phase stability under DRM and is consistent with the catalytic data showing sustained activity. However, a weak additional peak appears at ~77° in all patterns (including post-test materials). This reflection is assigned to the α-quartz packing (quartz wool) used to hold the powder bed and does not arise from catalyst evolution. Apart from this quartz contribution, no systematic peak growth in the 36–38°, 43–45°, or 59–66° regions was detected, i.e., no signatures of NiO/CoO or spinel formation within detection limits. Taken together, the XRD results support that the catalysts remain predominantly metallic during operation, while the small positive shift observed for CoNi reflects lattice/strain differences relative to Raney-Ni rather than the emergence of new crystalline phases. This finding suggests that CO_2 activation proceeded efficiently on CoNi sites, preventing extensive oxidation and maintaining surfaces available for CO_2 adsorption. Together with Raman evidence of reduced carbon deposition, these results support the view that CoNi promotes a continuous carbon–oxygen balance through enhanced CO_2 dissociation and in-situ gasification.

Taken together, the post-reaction SEM/EDS, Raman and XRD data indicate that the superior performance of the CoNi–Raney-Ni composites arises from a bifunctional, interfacial mechanism. Raney-Ni's high-area skeletal network efficiently activates CH_4 but tends to accumulate C* via methane decomposition ($CH_4 \rightarrow C^* + 2H_2$). CoNi, in contrast, preferentially activates CO_2, generating O* (or CO_x* species) that react with carbon on neighboring Ni sites ($C^* + O^* \rightarrow CO$), thereby removing surface carbon and regenerating Ni active sites. In the composite, CH_4 activation occurs mainly on Raney-Ni, CO_2 activation on CoNi, and O* spillover across CoNi|Ni contacts closes a catalytic carbon-gasification loop. This interfacial cooperation accounts for the sustained CH_4/CO_2 conversions and slower deactivation observed over time, as well as the shift of H_2/CO toward unity relative to pure Raney-Ni (enhanced CO

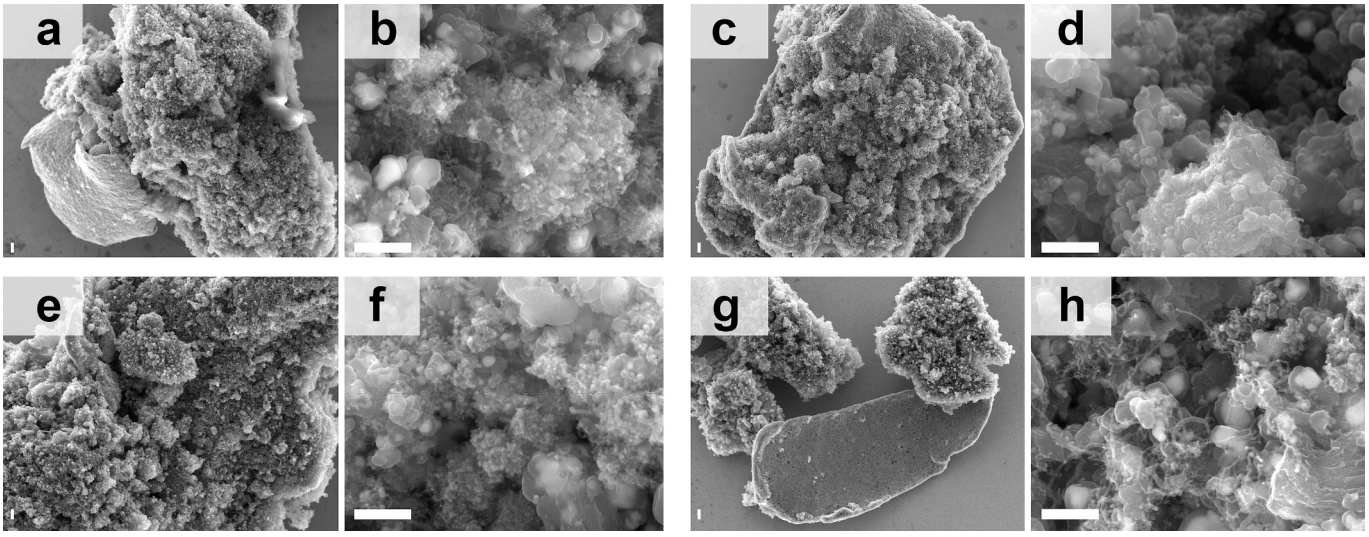

Fig. 4. FE-SEM micrographs of spent composite catalysts (a-b) C1, (c-d) C2, (e-f) C3, and (g-h) C4. Scale bar: 100 nm.

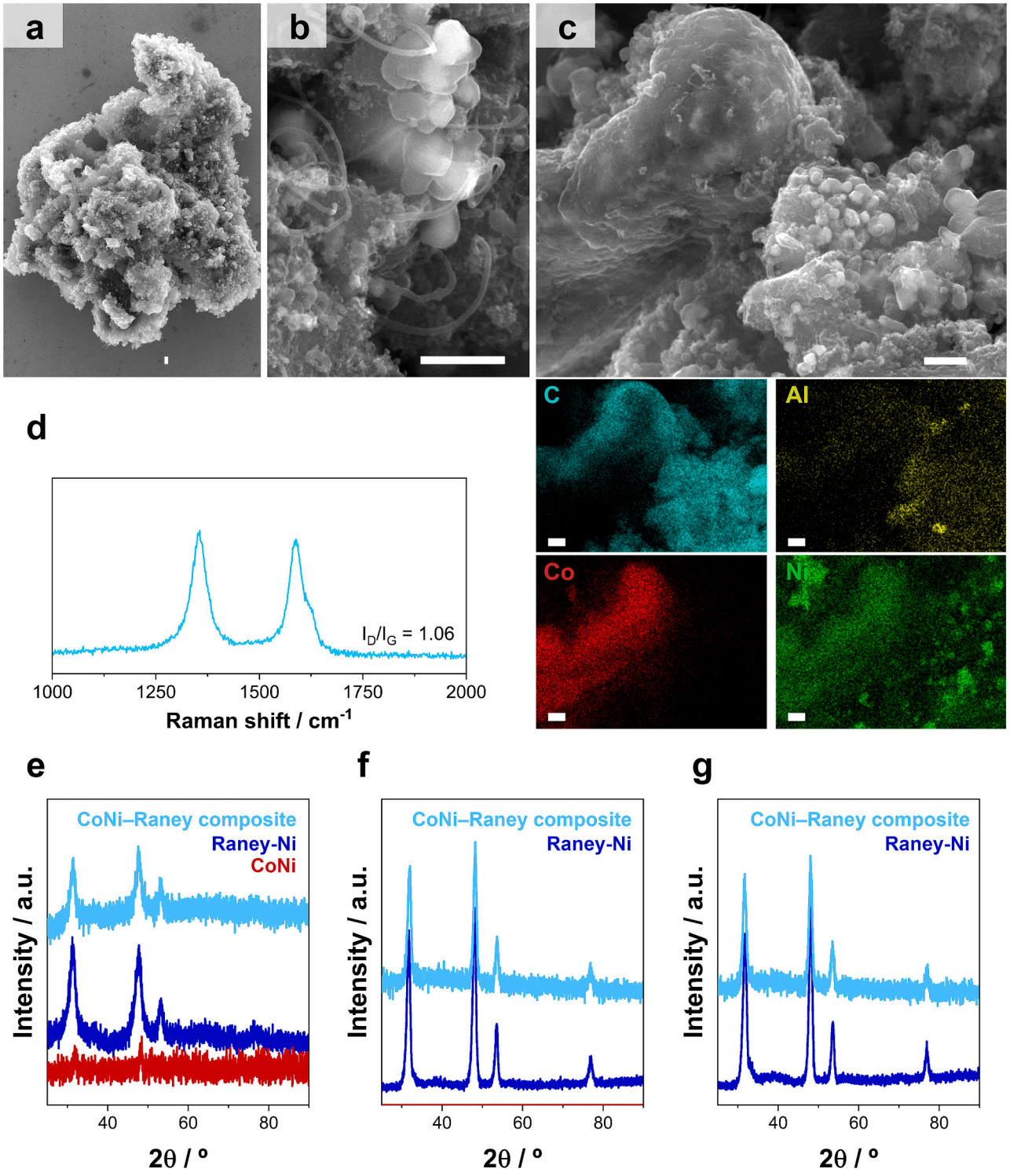

Fig. 5. Post-reaction characterization of the spent C4 catalyst: (a–c) FE-SEM micrographs at different magnifications. (c, bottom panel) EDS elemental mapping highlighting the distribution of key elements. Scale bar = 1 μm. (d) Raman spectra of the C4 catalyst after the stability test, indicating the carbon structure and degree of graphitization. XRD patterns of (e) fresh CoNi, Raney-Ni, and CoNi–Raney Ni composite catalysts; (f) Raney-Ni and CoNi–Raney Ni composite after five temperature-programmed DRM cycles; and (g) Raney Ni and CoNi–Raney Ni composite after stability testing.

formation on CoNi and mitigation of parallel methane cracking).

The synergy is composition-dependent. At intermediate CoNi loadings (~35–50 wt%), the interfacial density is sufficient to supply O* rapidly without unduly diluting the Ni sites required for CH_4 activation, yielding the optimal balance of activity, selectivity, and stability. Too little CoNi under-supplies O* (insufficient coke removal); too much CoNi reduces the effective Ni site density (rate limitation). This volcano-type trend aligns with the characterization results—lower Raman D/G ratios, fewer filamentous deposits in SEM, and more stable conversions—for the optimally loaded composites compared with either component alone, supporting a cooperative CoNi↔Ni redox interplay at the composite interfaces as the origin of the performance enhancement. This

synergistic interaction reduces carbon crystallinity and extends catalyst life, supporting the viability of CoNi–Raney-Ni composites for stable biogas reforming applications.

4. Conclusions

This study sets out to improve the catalytic efficiency and stability of Raney-Ni for methane dry reforming (DRM) under biogas-relevant conditions by incorporating electrochemically engineered CoNi microparticles as co-catalysts. Raney-Ni alone exhibited high intrinsic activity, achieving CH_4 conversions above 92 % at 700 °C and favorable H_2/CO ratios, confirming its potential as a non-noble metal catalyst for DRM. However, prolonged operation led to catalyst deactivation, primarily due to the formation of filamentous and graphitic carbon and particle sintering. This behavior limited the long-term viability of Raney-Ni under realistic continuous operation, especially in decentralized biogas upgrading settings.

To overcome these limitations, CoNi microparticles were synthesized via potentiostatic electrodeposition under optimized conditions and blended with Raney-Ni to form composite catalysts with varying CoNi loadings. Among the compositions tested, the 25 wt% CoNi–Raney-Ni catalyst (C4) showed the best balance between activity, syngas selectivity, and operational stability. This composite retained high CH_4 and CO_2 conversions (>90 %) and exhibited a stable H_2/CO ratio (~1.0) over extended periods. Compared to Raney-Ni alone, the CoNi–Raney-Ni composite catalysts displayed improved resistance to carbon deposition and thermal sintering, attributed to the synergistic roles of Ni and Co: while Raney-Ni provided high methane activation, CoNi promoted CO_2 dissociation and likely facilitated in-situ gasification of surface carbon species.

Post-reaction characterization confirmed the beneficial structural effects of CoNi incorporation. FE-SEM analyses of spent catalysts showed reduced particle agglomeration and less filamentous carbon growth in CoNi-containing systems. Raman spectroscopy supported these findings, indicating a lower degree of graphitization and higher D/G intensity ratios in the presence of CoNi, particularly in C1–C3 formulations. Furthermore, spatial mapping revealed that carbon deposition occurred preferentially on Raney-Ni domains, while CoNi regions remained relatively clean, suggesting localized carbon oxidation and removal facilitated by cobalt's oxygen affinity.

This work demonstrates that the strategic integration of an electrochemically tailored CoNi co-catalyst into a Raney-Ni matrix offers a scalable and cost-effective pathway toward durable DRM catalysts. The approach addresses key deactivation pathways – coking and sintering – without compromising catalytic activity, enabling sustained performance under thermochemically harsh conditions. These findings contribute a practical and mechanistically supported design strategy to the broader field of CO_2 valorization and biogas reforming.

Future work will focus on in-depth mechanistic studies using operando spectroscopy and isotopic tracing to elucidate the precise roles of Co and Ni in carbon oxidation and CoNi interfacial behavior. Additionally, long-term testing with real biogas mixtures, including H_2S and moisture, will be critical for assessing catalyst robustness under practical conditions. Finally, the electrochemical synthesis route offers flexibility for further compositional tuning and could be extended to both other compositions or bimetallic systems for broader catalytic applications in reforming and hydrogen production.

CRediT authorship contribution statement

Judit Lloreda: Writing – original draft, Methodology, Investigation, Formal analysis, Conceptualization. **Isabel Serrano:** Supervision, Resources, Investigation, Data curation. **Jordi Llorca:** Writing – review & editing, Validation, Supervision, Project administration, Funding acquisition, Formal analysis, Conceptualization. **Vanessa Abad:** Writing – review & editing, Visualization, Validation, Supervision, Resources, Project administration, Funding acquisition, Data curation, Conceptualization. **Elvira Gómez:** Writing – review & editing, Writing – original draft, Visualization, Validation, Supervision, Project administration, Funding acquisition, Formal analysis, Data curation, Conceptualization. **Albert Serrà:** Writing – review & editing, Writing – original draft, Visualization, Validation, Supervision, Project administration, Funding acquisition, Data curation, Conceptualization.

Declaration of competing interest

Authors declare no conflict of interest.

Acknowledgements

This work was supported by the Industrial Doctorates Program of the Department of Research and Universities (AGAUR) of the Generalitat de Catalunya (project 2022 DI 00035) and grant TED2021-129898B-C22, funded by Next Generation EU and MICIU/AEI/10.13039/501100011033. JL is a Serra Húnter Fellow and is grateful to MICIN/FEDER projects PID2021–124572OB-C31 and CEX2023-001300-M. Authors thank the CCiT-UB for the use of their equipment.

Appendix A. Supplementary data

Supplementary data to this article can be found online at https://doi.org/10.1016/j.cej.2025.169029.

Data availability

Data will be made available on request.

References

[1] S.F. Ahmed, M. Mofijur, S. Nuzhat, N. Rafa, A. Musharrat, S.S. Lam, A. Boretti, Sustainable hydrogen production: Technological advancements and economic analysis, Int. J. Hydrog. Energy 47 (2022) 37227–37255, https://doi.org/10.1016/j.ijhydene.2021.12.029.

[2] B.S. Zainal, P.J. Ker, H. Mohamed, H.C. Ong, I.M.R. Fattah, S.M.A. Rahman, L. D. Nghiem, T.M.I. Mahlia, Recent advancement and assessment of green hydrogen production technologies, Renew. Sust. Energ. Rev. 189 (2024) 113941, https://doi.org/10.1016/j.rser.2023.113941.

[3] C. Gunathilake, I. Soliman, D. Panthi, P. Tandler, O. Fatani, N.A. Ghulamullah, D. Marasinghe, M. Farhath, T. Madhujith, K. Conrad, Y. Du, M. Jaroniec, A comprehensive review on hydrogen production, storage, and applications, Chem. Soc. Rev. 53 (2024) 10900–10969, https://doi.org/10.1039/D3CS00731F.

[4] M. Aravindan, V. Madhan Kumar, V.S. Hariharan, T. Narahari, P. Arun Kumar, K. Madhesh, G. Praveen Kumar, R. Prabakaran, Fuelling the future: A review of non-renewable hydrogen production and storage techniques, Renew. Sust. Energ. Rev. 188 (2023) 113791, https://doi.org/10.1016/j.rser.2023.113791.

[5] M. Amin, H.H. Shah, A.G. Fareed, W.U. Khan, E. Chung, A. Zia, Z.U. Rahman Farooqi, C. Lee, Hydrogen production through renewable and non-renewable energy processes and their impact on climate change, Int. J. Hydrog. Energy 47 (2022) 33112–33134, https://doi.org/10.1016/j.ijhydene.2022.07.172.

[6] B. Panigrahy, K. Narayan, B. Ramachandra Rao, Green hydrogen production by water electrolysis: A renewable energy perspective, Mater Today Proc 67 (2022) 1310–1314, https://doi.org/10.1016/j.matpr.2022.09.254.

[7] C. Haoran, Y. Xia, W. Wei, Z. Yongzhi, Z. Bo, Z. Leiqi, Safety and efficiency problems of hydrogen production from alkaline water electrolyzers driven by renewable energy sources, Int. J. Hydrog. Energy 54 (2024) 700–712, https://doi.org/10.1016/j.ijhydene.2023.08.324.

[8] S. Vinardell, J.L. Cortina, C. Valderrama, Powering renewable hydrogen production with alternative water sources: Is it economically feasible? Energy Nexus 18 (2025) 100457 https://doi.org/10.1016/j.nexus.2025.100457.

[9] C. Bento, T.F. Lopes, P. Rodrigues, F. Gírio, C. Silva, Biogas reforming as a sustainable solution for hydrogen production: Comparative environmental metrics with steam-methane reforming and water electrolysis in the Portuguese context, Int. J. Hydrog. Energy 66 (2024) 661–675, https://doi.org/10.1016/j.ijhydene.2024.04.113.

[10] V. Abad, R. Avila, T. Vicent, X. Font, Promoting circular economy in the surroundings of an organic fraction of municipal solid waste anaerobic digestion treatment plant: Biogas production impact and economic factors, Bioresour. Technol. 283 (2019) 10–17, https://doi.org/10.1016/j.biortech.2019.03.064.

[11] P.G. Kougias, I. Angelidaki, Biogas and its opportunities—A review, Front. Environ. Sci. Eng. 12 (2018) 14, https://doi.org/10.1007/s11783-018-1037-8.

[12] A. Calbry-Muzyka, H. Madi, F. Rüsch-Pfund, M. Gandiglio, S. Biollaz, Biogas composition from agricultural sources and organic fraction of municipal solid

waste, Renew. Energy 181 (2022) 1000–1007, https://doi.org/10.1016/j.renene.2021.09.100.
[13] M.K. Jameel, M.A. Mustafa, H.S. Ahmed, A.J. Mohammed, H. Ghazy, M.N. Shakir, A.M. Lawas, S.K. Mohammed, A.H. Idan, Z.H. Mahmoud, H. Sayadi, E. Kianfar, Biogas: Production, properties, applications, economic and challenges: A review, Results Chem. 7 (2024) 101549, https://doi.org/10.1016/j.rechem.2024.101549.
[14] J. Colón, E. Cadena, A.B. Colazo, R. Quirós, A. Sánchez, X. Font, A. Artola, Toward the implementation of new regional biowaste management plans: environmental assessment of different waste management scenarios in Catalonia, Resour. Conserv. Recycl. 95 (2015) 143–155, https://doi.org/10.1016/j.resconrec.2014.12.012.
[15] C. Vlachokostas, C. Achillas, V. Diamantis, A.V. Michailidou, K. Baginetas, D. Aidonis, Supporting decision making to achieve circularity via a biodegradable waste-to-bioenergy and compost facility, J. Environ. Manag. 285 (2021) 112215, https://doi.org/10.1016/j.jenvman.2021.112215.
[16] Agència de Residus de Catalunya, Informe anual de la generació i gestió dels residus municipals 2023, Generalitat de Catalunya (2024). https://estadistiques.arc.cat/ARC/ (accessed May 20, 2025).
[17] B. Agún, A. Abánades, Comprehensive review on dry reforming of methane: Challenges and potential for greenhouse gas mitigation, Int. J. Hydrog. Energy 103 (2025) 395–414, https://doi.org/10.1016/j.ijhydene.2025.01.160.
[18] A.M. Alhassan, I. Hussain, O.A. Taialla, M.M. Awad, A. Tanimu, K. Alhooshani, S. A. Ganiyu, Advances in catalytic dry reforming of methane (DRM): Emerging trends, current challenges, and future perspectives, J. Clean. Prod. 423 (2023) 138638, https://doi.org/10.1016/j.jclepro.2023.138638.
[19] Z. Alipour, V. Babu Borugadda, H. Wang, A.K. Dalai, Syngas production through dry reforming: A review on catalysts and their materials, preparation methods and reactor type, Chem. Eng. J. 452 (2023) 139416, https://doi.org/10.1016/j.cej.2022.139416.
[20] J. Li, C. Qin, Z. Lv, C. Gao, L. Chen, S. Xu, Techno-economic analysis of integrated carbon capture and dry reforming of methane, Energy 316 (2025) 134516, https://doi.org/10.1016/j.energy.2025.134516.
[21] S.B. Jo, J.H. Woo, J.H. Lee, T.Y. Kim, H.I. Kang, S.C. Lee, J.C. Kim, CO2 green technologies in CO_2 capture and direct utilization processes: methanation, reverse water-gas shift, and dry reforming of methane, Sustain. Energy Fuels 4 (2020) 5543–5549, https://doi.org/10.1039/d0se00951b.
[22] R.-Y. Chein, W.-H. Chen, H. Chyuan Ong, P. Loke Show, Y. Singh, Analysis of methanol synthesis using CO_2 hydrogenation and syngas produced from biogas-based reforming processes, Chem. Eng. J. 426 (2021) 130835, https://doi.org/10.1016/j.cej.2021.130835.
[23] W. Jung, G.B. Rhim, K.Y. Kim, M.H. Youn, D.H. Chun, J. Lee, Comprehensive analysis of syngas-derived Fischer–Tropsch synthesis using iron-based catalysts with varied acidities, Chem. Eng. J. 484 (2024) 149408, https://doi.org/10.1016/j.cej.2024.149408.
[24] M. Corda, O. Vovk, M. Marinova, T. Len, V.A. Kondratenko, E.V. Kondratenko, V. V. Ordomsky, A.Y. Khodakov, Syngas conversion to light olefins over silver metallic nanoparticles in bifunctional catalysts, Chem. Eng. J. 506 (2025) 159700, https://doi.org/10.1016/j.cej.2025.159700.
[25] B. Ruscic, Active Thermochemical Tables: Sequential Bond Dissociation Enthalpies of Methane, Ethane, and Methanol and the Related Thermochemistry, J. Phys. Chem. A 119 (2015) 7810–7837, https://doi.org/10.1021/acs.jpca.5b01346.
[26] O.U. Osazuwa, K.H. Ng, An overview on the carbon deposited during dry reforming of methane (DRM): Its formation, deposition, identification, and quantification, Res. Eng. Des. 25 (2025) 104328, https://doi.org/10.1016/j.rineng.2025.104328.
[27] M.H. Amin, S. Putla, S. Bee Abd Hamid, S.K. Bhargava, Understanding the role of lanthanide promoters on the structure–activity of nanosized Ni/γ-Al_2O_3 catalysts in carbon dioxide reforming of methane, Appl. Catal., A 492 (2015) 160–168, https://doi.org/10.1016/j.apcata.2014.12.038.
[28] T.W. Hansen, A.T. DeLaRiva, S.R. Challa, A.K. Datye, Sintering of Catalytic Nanoparticles: Particle Migration or Ostwald Ripening? Acc. Chem. Res. 46 (2013) 1720–1730, https://doi.org/10.1021/ar3002427.
[29] N.A.K. Aramouni, J.G. Touma, B.A. Tarboush, J. Zeaiter, M.N. Ahmad, Catalyst design for dry reforming of methane: Analysis review, Renew. Sust. Energ. Rev. 82 (2018) 2570–2585, https://doi.org/10.1016/j.rser.2017.09.076.
[30] F. Yu, X. Tao, H. Yu, T. Zhao, M. Li, L. Liu, H. Wang, Enhancing the sintering stability of NiCo/CeO_2-Al_2O_3 catalyst in dry reforming of methane by shaping the Ostwald ripening diffusion path, Chem. Eng. J. 504 (2025) 158725, https://doi.org/10.1016/j.cej.2024.158725.
[31] D.G. Araiza, D.G. Arcos, A. Gómez-Cortés, G. Díaz, Dry reforming of methane over Pt-Ni/CeO_2 catalysts: Effect of the metal composition on the stability, Catal. Today 360 (2021) 46–54, https://doi.org/10.1016/j.cattod.2019.06.018.
[32] J.W. Han, C. Kim, J.S. Park, H. Lee, Highly Coke-Resistant Ni Nanoparticle Catalysts with Minimal Sintering in Dry Reforming of Methane, ChemSusChem 7 (2014) 451–456, https://doi.org/10.1002/cssc.201301134.
[33] J. Zhang, F. Li, Coke-resistant Ni@SiO_2 catalyst for dry reforming of methane, Appl. Catal. B 176–177 (2015) 513–521, https://doi.org/10.1016/j.apcatb.2015.04.039.
[34] Z. Bian, S. Das, M.H. Wai, P. Hongmanorom, S. Kawi, A Review on Bimetallic Nickel-Based Catalysts for CO_2 Reforming of Methane, ChemPhysChem 18 (2017) 3117–3134, https://doi.org/10.1002/cphc.201700529.
[35] H. Zhu, H. Chen, M. Zhang, C. Liang, L. Duan, Recent advances in promoting dry reforming of methane using nickel-based catalysts, Catal. Sci. Technol. 14 (2024) 1712–1729, https://doi.org/10.1039/d3cy01612a.
[36] P. Frontera, A. Macario, A. Aloise, P.L. Antonucci, G. Giordano, J.B. Nagy, Effect of support surface on methane dry-reforming catalyst preparation, Catal. Today 218–219 (2013) 18–29, https://doi.org/10.1016/j.cattod.2013.04.029.
[37] M. Armengol-Profitós, A. Braga, L. Pascua-Solé, I. Lucentini, X. Garcia, L. Soler, X. Vendrell, I. Serrano, I.J. Villar-Garcia, V. Pérez-Dieste, C. Escudero, N.J. Divins, J. Llorca, Enhancing the performance of a novel CoRu/CeO_2 bimetallic catalyst for the dry reforming of methane via a mechanochemical process, Appl Catal B 345 (2024) 123624, https://doi.org/10.1016/j.apcatb.2023.123624.
[38] S. Fazlikeshteli, X. Vendrell, J. Llorca, Catalytic partial oxidation of methane over bimetallic Ru–Ni supported on CeO_2 for syngas production, Int. J. Hydrog. Energy 51 (2024) 1494–1507, https://doi.org/10.1016/j.ijhydene.2023.07.349.
[39] A. Braga, M. Armengol-Profitós, L. Pascua-Solé, X. Vendrell, L. Soler, I. Serrano, I. J. Villar-Garcia, V. Pérez-Dieste, N.J. Divins, J. Llorca, Bimetallic NiFe Nanoparticles Supported on CeO_2 as Catalysts for Methane Steam Reforming, ACS Appl. Nano Mater. 6 (2023) 7173–7185, https://doi.org/10.1021/acsanm.3c00104.
[40] O. Muraza, A. Galadima, A review on coke management during dry reforming of methane: Revisiting coke management in dry reforming of methane, Int. J. Energy Res. 39 (2015) 1196–1216, https://doi.org/10.1002/er.3295.
[41] Y. Kathiraser, U. Oemar, E.T. Saw, Z. Li, S. Kawi, Kinetic and mechanistic aspects for CO_2 reforming of methane over Ni based catalysts, Chem. Eng. J. 278 (2015) 62–78, https://doi.org/10.1016/j.cej.2014.11.143.
[42] R. Bujaldón, A. Fons, J. Garcia-Amorós, C. Vaca, J. Nogués, M.J. Esplandiu, E. Gómez, B. Sepúlveda, A. Serrà, Minimizing energy demand in the conversion of levulinic acid to γ-valerolactone via photothermal catalysis using Raney Ni, Adv. Sci. (2025) 2416153, https://doi.org/10.1002/advs.202416153.
[43] Z. Sun, Z.-H. Zhang, T.-Q. Yuan, X. Ren, Z. Rong, Raney Ni as a Versatile Catalyst for Biomass Conversion, ACS Catal. 11 (2021) 10508–10536, https://doi.org/10.1021/acscatal.1c02433.
[44] A.F. Cunha, J.J.M. Órfão, J.L. Figueiredo, Methane decomposition on Ni–Cu alloyed Raney-type catalysts, Int. J. Hydrog. Energy 34 (2009) 4763–4772, https://doi.org/10.1016/j.ijhydene.2009.03.040.
[45] A.F. Cunha, J.J.M. Órfão, J.L. Figueiredo, Catalytic decomposition of methane on Raney-type catalysts, Appl. Catal., A 348 (2008) 103–112, https://doi.org/10.1016/j.apcata.2008.06.028.
[46] V. Dal Santo, A. Gallo, A. Naldoni, M. Guidotti, R. Psaro, Bimetallic heterogeneous catalysts for hydrogen production, Catal. Today 197 (2012) 190–205, https://doi.org/10.1016/j.cattod.2012.07.037.
[47] Y. Sun, Y. Zhang, X. Yin, C. Zhang, Y. Li, J. Bai, Recent advances in the design of high-performance cobalt-based catalysts for dry reforming of methane, Green Chem. 26 (2024) 5103–5126, https://doi.org/10.1039/d3gc05136f.
[48] S. Chen, J. Zaffran, B. Yang, Dry reforming of methane over the cobalt catalyst: Theoretical insights into the reaction kinetics and mechanism for catalyst deactivation, Appl Catal B 270 (2020) 118859, https://doi.org/10.1016/j.apcatb.2020.118859.
[49] D. Pakhare, J. Spivey, A review of dry (CO_2) reforming of methane over noble metal catalysts, Chem. Soc. Rev. 43 (2014) 7813–7837, https://doi.org/10.1039/c3cs60395d.
[50] J. Horlyck, C. Lawrey, E.C. Lovell, R. Amal, J. Scott, Elucidating the impact of Ni and Co loading on the selectivity of bimetallic NiCo catalysts for dry reforming of methane, Chem. Eng. J. 352 (2018) 572–580, https://doi.org/10.1016/j.cej.2018.07.009.
[51] D. San-José-Alonso, J. Juan-Juan, M.J. Illán-Gómez, M.C. Román-Martínez, Ni, Co and bimetallic Ni–Co catalysts for the dry reforming of methane, Appl. Catal., A 371 (2009) 54–59, https://doi.org/10.1016/j.apcata.2009.09.026.
[52] E. Gómez, E. Vallés, Electrodeposition of Co + Ni alloys on modified silicon substrates, J. Appl. Electrochem. 29 (1999) 803–810, https://doi.org/10.1023/a:1003580302490.
[53] E. Gómez, E. Vallés, Thick cobalt coatings obtained by electrodeposition, J. Appl. Electrochem. 32 (2002) 693–700, https://doi.org/10.1023/a:1020194532136.
[54] C.B. Rodella, G. Kellermann, M.S.P. Francisco, M.H. Jordão, D. Zanchet, Textural and Structural Analyses of Industrial Raney Nickel Catalyst, Ind. Eng. Chem. Res. 47 (2008) 8612–8618, https://doi.org/10.1021/ie800543t.
[55] C. Jensen, M.S. Duyar, Thermodynamic Analysis of Dry Reforming of Methane for Valorization of Landfill Gas and Natural Gas, Energy Tech. 9 (2021) 2100106, https://doi.org/10.1002/ente.202100106.
[56] Y. Xue, L. Xu, M. Chen, C. Wu, G. Cheng, N. Wang, X. Hu, Constructing Ni-based confinement catalysts with advanced performances toward the CO_2 reforming of CH_4 : state-of-the-art review and perspectives, Catal. Sci. Technol. 11 (2021) 6344–6368, https://doi.org/10.1039/D1CY01039E.
[57] Q. Zhao, L. Bao, H. Wang, D. Dou, Y. Cong, C. Li, Bimetallic Co–Ni alloy nanoparticles loaded on nitrogen-doped wrinkled carbon nanospheres as high-performance bifunctional ORR/OER electrocatalyst in alkaline media, Ionics 30 (2024) 4797–4810, https://doi.org/10.1007/s11581-024-05478-5.
[58] J. Sasson Bitters, T. He, E. Nestler, S.D. Senanayake, J.G. Chen, C. Zhang, Utilizing bimetallic catalysts to mitigate coke formation in dry reforming of methane, J. Energy Chem. 68 (2022) 124–142, https://doi.org/10.1016/j.jechem.2021.11.041.